biosensors

MDPI

Article

Defect-Engineering of 2D Dichalcogenide VSe_2 to Enhance Ammonia Sensing: Acumens from DFT Calculations

Gopal Sanyal [1], Surinder Pal Kaur [2], Chandra Sekhar Rout [3] and Brahmananda Chakraborty [4,5,*]

[1] Mechanical Metallurgy Division, Bhabha Atomic Research Centre, Trombay, Mumbai 400085, India
[2] Department of Chemistry, Indian Institute of Technology Ropar, Rupnagar 140001, India
[3] Centre for Nano and Material Sciences, Jain Global Campus, Jakkasandra, Ramanagaram, Bangalore 562112, India
[4] High Pressure and Synchroton Radiation Physics Division, Bhabha Atomic Research Centre, Trombay, Mumbai 400085, India
[5] Homi Bhabha National Institute, Mumbai 400094, India
* Correspondence: brahma@barc.gov.in

Abstract: Opportune sensing of ammonia (NH_3) gas is industrially important for avoiding hazards. With the advent of nanostructured 2D materials, it is felt vital to miniaturize the detector architecture so as to attain more and more efficacy with simultaneous cost reduction. Adaptation of layered transition metal dichalcogenide as the host may be a potential answer to such challenges. The current study presents a theoretical in-depth analysis regarding improvement in efficient detection of NH_3 using layered vanadium di-selenide (VSe_2) with the introduction of point defects. The poor affinity between VSe_2 and NH_3 forbids the use of the former in the nano-sensing device's fabrications. The adsorption and electronic properties of VSe_2 nanomaterials can be tuned with defect induction, which would modulate the sensing properties. The introduction of Se vacancy to pristine VSe_2 was found to cause about an eight-fold increase (from −012 eV to −0.97 eV) in adsorption energy. A charge transfer from the N 2p orbital of NH_3 to the V 3d orbital of VSe_2 has been observed to cause appreciable NH_3 detection by VSe_2. In addition to that, the stability of the best-defected system has been confirmed through molecular dynamics simulation, and the possibility of repeated usability has been analyzed for calculating recovery time. Our theoretical results clearly indicate that Se-vacant layered VSe_2 can be an efficient NH_3 sensor if practically produced in the future. The presented results will thus potentially be useful for experimentalists in designing and developing VSe_2-based NH_3 sensors.

Keywords: 2D materials; VSe_2 monolayer; ammonia sensing; electronic properties; reversible sensors; density functional theory

Citation: Sanyal, G.; Kaur, S.P.; Rout, C.S.; Chakraborty, B. Defect-Engineering of 2D Dichalcogenide VSe_2 to Enhance Ammonia Sensing: Acumens from DFT Calculations. *Biosensors* **2023**, *13*, 257. https://doi.org/10.3390/bios13020257

Received: 4 December 2022
Revised: 7 February 2023
Accepted: 10 February 2023
Published: 11 February 2023

1. Introduction

With the development of technology, the requirement for gas sensors in the fields of industry, agriculture, medicine, air-quality monitoring, etc., has been amplified [1,2]. For instance, gases such as carbon monoxide, nitrogen oxide, nitrogen dioxide, ammonia, etc. are harmful to living beings and can trigger serious health issues [3,4]. To eliminate such hazardous gases from the environment, lucrative sensors with good stability, sensitivity, and selectivity are desirable. In the past, metal oxides such as ZnO, SnO_2, and so on were explored as efficient sensors having good sensitivity and selectivity towards the sensing of harmful gases [5]. Although metal oxides are cheaper and need low fabrication costs, their elevated operating temperature restricts their use in sensing devices [6]. Following this, various types of sensing materials have been reported in the past. Among all the reported sensing materials, chemi-resistors are recommended as promising sensitive and selective sensors [7,8]. For instance, Oudenhoven et al. reported a thin layer of ionic liquid

[BMIM][NTf_2] as the electrolyte, capable of sensing NH_3 even at a level of 1 ppm [9]. On the other hand, Amirjani et al. reported a calorimetric sensor for detecting NH_3 by utilizing localized surface plasmon resonance of Ag nanoparticles for detection in the range of 10–1000 mg L^{-1} [10]. The electrochemical sensor developed by Arya et al. uses SnO_2 nanoparticles synthesized with the sol–gel route to sense NH_3 in aqueous solution [11].

Graphene is a two-dimensional carbon allotrope with a zero band gap and possesses a high surface-to-volume ratio [12,13]. The discovery of graphene brought a breakthrough in the exploration of two-dimensional nanomaterials [14–18]. Due to the presence of novel physical and chemical properties, two-dimensional nanomaterials can be used in a wide range of applications such as energy storage devices, catalysis, sensing devices, etc. [19–21]. The application of two-dimensional materials, namely borophene, phosphorene, transition metal dichalcogenides (TMDs), etc., in gas sensing has been studied by different research groups [19–26]. For instance, honeycomb germanium is reported to act as an efficient sensor as compared to graphene-based sensors [27,28]. Sosa and his coworkers investigated the application of alkali, alkaline earth metals, and transition metal-doped germanene in ammonia (NH_3) sensing by computing adsorption energies, charge transfer analysis, work function, and desorption time [29]. Several other studies have also been reported in the past to investigate the adsorption properties of NH_3 on different two-dimensional materials [30]. For instance, adsorption energies and diffusion energy barriers were computed for NH_3 adsorption on MoO_3 nanomaterial by Xu and coworkers [31]. The authors reported the low sensing of NH_3 on the studied two-dimensional material. Lv and his coworkers studied the sensing properties of NH_3 on a two-dimensional C_3N monolayer by performing density functional theory [32].

Transition metal dichalcogenide nanosheet; $MoSe_2$ is reported to act as an efficient sensor in the sensing of CO, NO, NO, and NO_2 gases [33,34]. It is also possible to tune the physical and chemical properties of such two-dimensional nanomaterials by tuning their structures [35–43]. The Janus TMDs are two-dimensional nanomaterials in which a metal layer is sandwiched between two different non-metal atom layers. The difference in the non-metal atom layers introduces asymmetry, which is responsible for enhancing the physicochemical properties of such materials. The Janus TMDs have been explored for their use in hydrogen storage, catalysis, water splitting, etc. [44–47]. Along with these properties, the application of Janus TMDs in gas sensing has also been studied by researchers in the past [48–50]. For instance, the role of MoSSe nanomaterial in the sensing of CO, CO_2, NO, and NO_2 was studied using DFT methods [46]. The authors reported that the selectivity of sensing can be improved with the help of external strain. Following this, the sensing properties of the defected Janus TMDs have also been studied in the past [51]. The studies showed that the defected Janus TMDs showed higher sensitivity towards the gas molecules as compared to pristine monolayers.

The charge transfer between adsorbate and adsorbent partakes in the gas sensing mechanism (Figure 1). Previous studies showed that the gas-sensing behavior of two-dimensional can be improved by introducing p-type or n-type doping [52–55]. The doping can be introduced by incorporating impurities in the two-dimensional nanomaterial lattice [56,57]. Suh and his group reported the hole generation in the $MoSe_2$ monolayer with the doping of Nb in the lattice structure [58]. The gas-sensing behavior of Nb-doped MoS_2 nanosheets has been investigated by Choi and his coworkers [59]. Their report stated that optimum NO_2 sensing of MoS_2 can be enhanced up to 8% with Nb doping and hence, can be considered an effective way to achieve high-performance gas sensing devices. The improvement of the gas-sensing behavior of $MoSe_2$ and $MoTe_2$ nanomaterials with the elemental substitution is also reported in the past [60]. The role of V, Nb, and Ta-doped MoS_2 in NH_3, H_2O, and NO_2 sensing has been studied by Zhu and his group [61]. Authors suggested that doping of transition metal atoms enriches the sensing properties of MoS_2. The effect of Al, Si, and P-doped MoS_2 on the adsorption as well as sensing of NH_3 has been studied by Luo and his group [62]. The effect of nitrogen, phosphorus, and arsenic doping on the CO, NO, and HF sensing of Janus WSSe nanosheets has been studied in the past

using DFT methods [63]. The studies showed that ~3.12% doping of nitrogen, phosphorus, and arsenic makes Janus WSSe nanosheets efficient sensing materials even without imposing external strain. The utilization of VSe_2 nanomaterial for the sensing of nitrobenzene and catechol has been reported in past studies [64,65]. Vacancy engineering has been reviewed as a critical strategy for tuning electron and phonon structures of two-dimensional materials in general and for gas-sensing applications in particular [66–68]. For instance, in the case of TMDs, the introduction of vacancy has been reported to be beneficial for the sensing of SO_2, NH_3, NO_2, 'NO, O_2, and CO, and decomposed SF_6 gases in $SnSe_2$, SnS_2, MoS_2, $PtSe_2$, and WS_2 layered systems, respectively [69–73]. Keeping the above in mind, the potential of vacancy-engineered VSe_2 for the detection of NH_3 appears to be a still unaddressed topic, to the best knowledge of the authors.

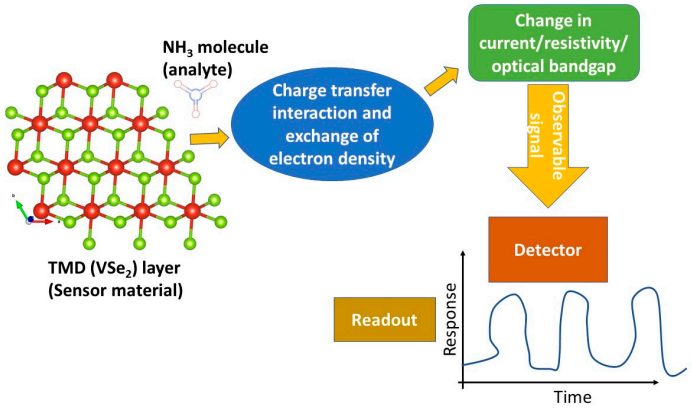

Figure 1. Schematic flow diagram of gas sensing mechanism involving charge transfer interactions.

The modality of detection of NH_3 with VSe_2 nanosheets has thus been theoretically studied in the present work. The effect of defect-engineered nanosheets has also been considered in this work by introducing V-defected as well as Se-defected layered VSe_2 nanomaterials. Using first-principles calculations, the change in the electronic and magnetic properties of defected VSe_2 monolayers has been compared with the pristine material. The sensing capabilities of pristine and defected VSe_2 monolayers have also been assessed in terms of adsorption energy values, electronic, magnetic, and charge transfer properties with the NH_3 molecule.

2. Computational Methods

The density functional theory (DFT) computations were accomplished by means of the Projector Augmented Wave (PAW) principles as implemented in the Vienna ab initio Simulation Package (VASP) [74–77]. In the simulations, generalized gradient approximation (GGA) was used for exchange-correlation functions [78]. During the computations, the convergence criteria for Hellman–Feynman forces were kept at 0.01 eV/Å alongside the plane wave cut-off energy of 600 eV. The long-range interactions may impact the sensing properties of the material. Hence, long-range interactions were taken care of with Grimme's DFT-D3 functional [79,80]. The Γ-centered K-points grid of $6 \times 6 \times 1$ was used for the integration of the first Brillouin zone [81]. A vacuum of 20 Å was introduced in the z-direction to avoid the interactions between the layers in the Z direction. The thermal stability of the VSe_2 monolayer adsorbed with NH_3 was computed with the help of ab-initio molecular dynamics simulations (AIMD). The AIMD simulations were carried out in the NVT ensemble using the Nosé–Hoover thermostat to determine the thermal stability of $VSe_2 + NH_3$ and $VSe_2(Se_v)$ + NH3 systems at 400 K. The simulations were carried out for a total time of 5 ps with a time step of 1 fs.

3. Results and Discussion

3.1. Structural Analysis of Pristine and Defected VSe_2

The 4 × 4 × 1 supercell of VSe_2 was used to mimic the two-dimensional monolayer in this work. The geometry-relaxed structure of pristine VSe_2 is shown in Figure 2a. In this structure, the metal atom layer is embedded between the selenium atom layers. Using the optimized structure of pristine VSe_2, V-defected VSe_2 was constructed by removing a single V-metal atom from the monolayer [Figure 2b]. Similarly, the Se-defected layer was modeled by eliminating a Se-atom from the monolayer [Figure 2c]. The V and Se-defected monolayers are described as $VSe_2(V_v)$ and $VSe_2(Se_v)$, distinctly. The optimized structures of VSe_2, $VSe_2(V_v)$, and $VSe_2(Se_v)$ are used for the further adsorption of the NH_3 molecule at various possible positions, as mentioned below.

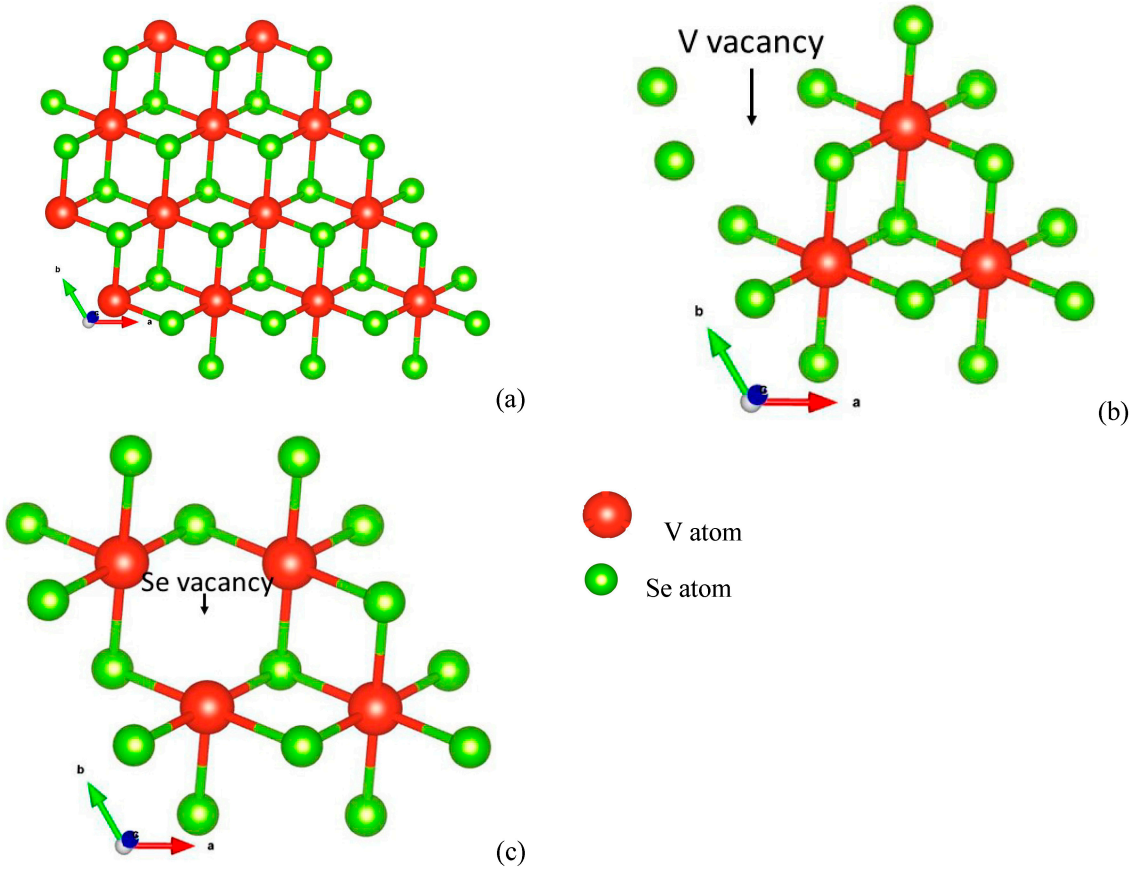

Figure 2. Relaxed structure of (**a**) pristine VSe_2, (**b**) VSe_2 deficient with V atom, and (**c**) VSe_2 deficient with Se atom.

3.2. Adsorption of NH_3 on VSe_2, $VSe_2(V_v)$, and $VSe_2(Se_v)$

To understand the NH_3 sensing of pure and defected VSe_2, the NH_3 molecule was placed at various possible sites, 2 Å above the VSe_2, $VSe_2(V_v)$, and $VSe_2(Se_v)$ monolayers. The structurally relaxed geometries upon NH_3 introduction on VSe_2, $VSe_2(V_v)$, and $VSe_2(Se_v)$ monolayers are depicted in Figure 3. The stability of the NH_3 adsorbed complexes is assessed in terms of adsorption energy values both with and without van der Waals (VdW) interactions.

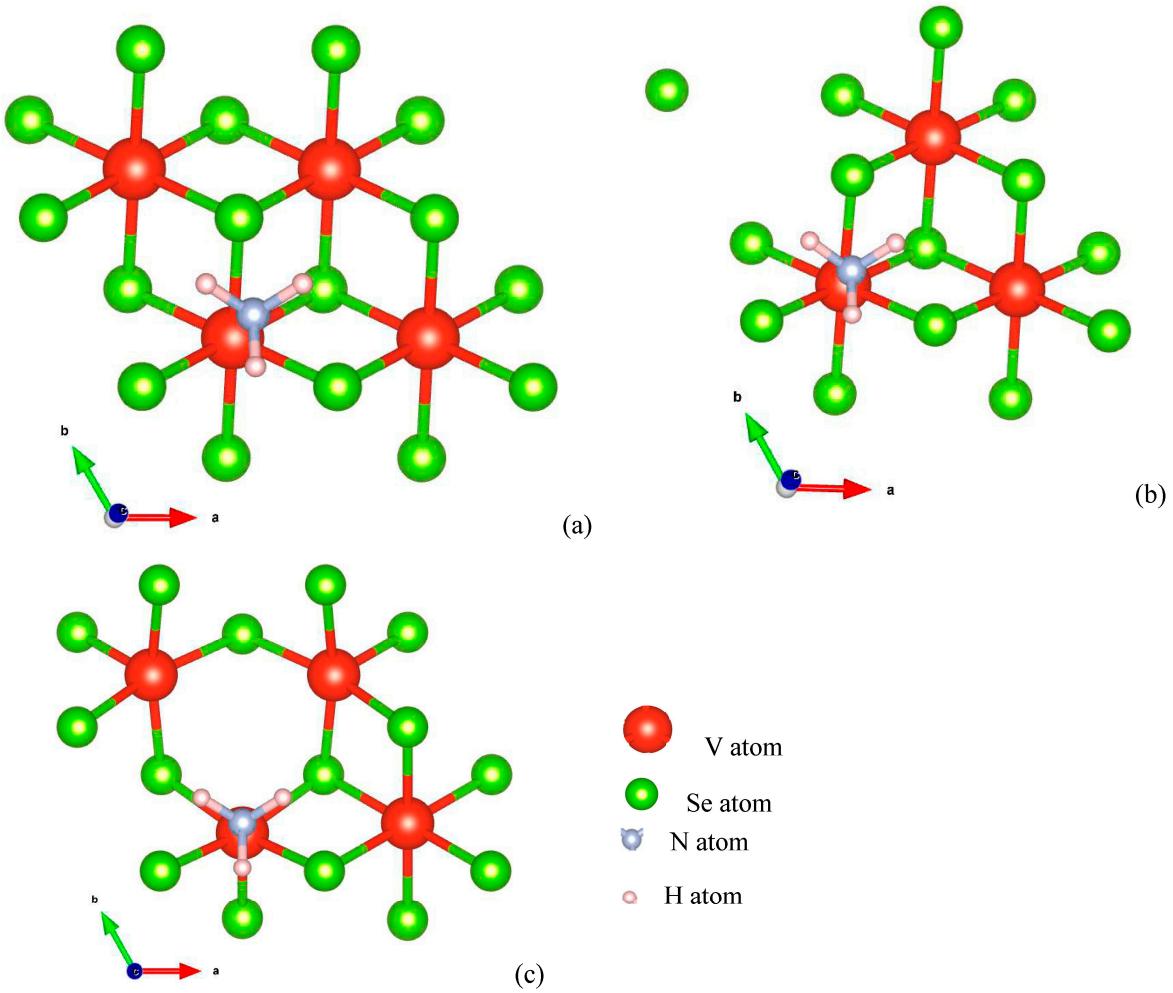

Figure 3. Relaxed structures of (**a**) NH_3 (N atom directly placed above V atom) on pristine VSe_2, (**b**) NH_3 (N atom directly placed above V atom) on VSe_2 deficient with V atom, and (**c**) NH_3 (N atom directly placed above V atom) on VSe_2 deficient with Se atom.

The adsorption energy is computed using the following equation:

$$BE = E_{(complex)} - E_{(monolayer)} - E_{(NH3)} \quad (1)$$

In this equation, $E_{(complex)}$ is the energy of the NH_3 adsorbed VSe_2/$VSe_2(V_v)$/$VSe_2(Se_v)$ systems. The $E_{(monolayer)}$ represents the energy of the VSe_2 or $VSe_2(V_v)$ or $VSe_2(Se_v)$ systems. The last term $E_{(NH3)}$ represents the energy of the isolated ammonia gas molecule.

The adsorption energy values are shown in Table 1. It can be observed from Table 1 that the NH_3 molecule is weakly bound to the pure VSe_2. Or, in other words, the NH_3 shows weak affinity towards the VSe_2 monolayer, specifying that pure material is not much suitable for sensing purposes. The result shown in Table 1 for the VSe_2+NH_3 system corresponds to the adsorption energy of 0.124 eV for the case when the N atom of NH_3 has been placed upright the V atom of VSe_2. The same practice has been repeated for the other three possible sites, i.e., Se atom, V-Se bond, and center of a hexagonal ring consisting of V and Se atoms, and all four obtained adsorption energy values are shown in Table S1. As can be seen, the adsorption energy for the arrangement corresponding to the "above V" case is the least (though positive without VdW incorporation); further, all calculations are based on that arrangement. However, $VSe_2(V_v)$ and $VSe_2(Se_v)$ monolayers show stronger affinity towards NH_3 with adsorption energy values of −0.22 and −0.66 eV, respectively. The present studies also determined the influence of long-range interactions by computing the adsorption energy values with DFT-D3 functional to consider van der Waal interaction. It can be observed from Table 1 that the adsorption energy values

improve with the inclusion of VdW interactions. The values reported in Table 1 suggest that the VSe_2(Sev) + NH_3 forms the most stable complex due to higher adsorption energy values. The bond lengths between NH_3 and the adsorbent are also measured and are given in Table 1. In the case of VSe_2(Sev) + NH_3, the distance between the vanadium atom of the monolayer and the N atom of NH_3 is reduced as compared to the VSe_2 + NH_3 complex. This supports stronger adsorption interactions between $VSe_2(Se_v)$ and the NH_3 molecule. As the $VSe_2(Se_v)$ + NH_3 forms the most stable complex, the change in the electronic properties of pure and Se-defected monolayers with the adsorption of NH_3 molecule is studied in this work and has been comparatively discussed further.

Table 1. Adsorption energies for the adsorption of NH_3 on VSe_2, $VSe_2(V_v)$, and $VSe_2(Se_v)$ systems with and without VdW functional. The bond lengths between the atoms of adsorbate and adsorbent are given in Å units.

System	Adsorption Energy (eV)	Bond Length (Å)
VSe_2 + NH_3	0.124	V-N: 4.786 S-N: 3.94
VSe_2 + NH_3 (with VdW)	−0.12	V-N: 4.709 S-N: 3.93
VSe_2 (V vacancy) + NH_3	−0.219	V-N: 4.756 S-N: 3.92
VSe_2 (V vacancy) + NH_3 (with VdW)	−0.342	V-N: 4.479 S-N: 3.732
VSe_2 (Se vacancy) + NH_3	−0.664	V-N: 2.26 S-N: 3.697
VSe_2 (Se vacancy) + NH_3 (with VdW)	−0.97	V-N: 2.253 S-N: 3.681
VSe_2 (2Se vacancy) + NH_3	−1.33	V-N: 2.242 S-N: 3.514
VSe_2 (2Se vacancy) + NH_3 (with VdW)	−1.58	V-N: 2.241 S-N: 3.501

To study the effect of a further increase in defect density, a VSe_2 structure deficient with two Se atoms has been relaxed and again optimized with the insertion of an NH_3 molecule. (Figure 4). The resultant adsorption energy values (−1.33 and −1.58 eV with VdW), as shown in Table 1, indicate stronger adsorption. Such observation is promising to conclude that doubling the Se vacancy population is beneficial for better NH_3 detection.

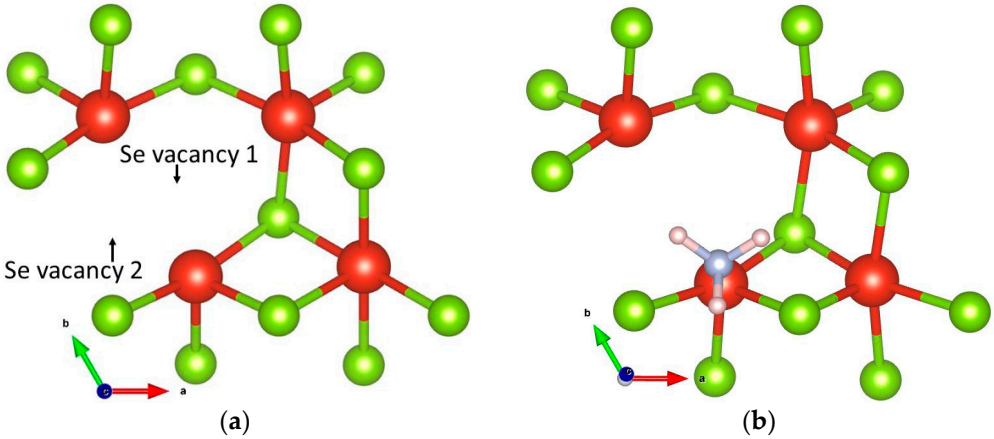

(**a**) (**b**)

Figure 4. Relaxed structures of (**a**) VSe_2 deficient with 2 Se atoms and (**b**) NH_3 (N atom directly placed above V atom) on VSe_2 deficient with 2 Se atoms.

3.3. Total Density of States (TDOS) Plots

In order to get insights regarding charge transfer and the interaction mechanism of NH_3 with pristine and defected VSe_2, we have presented total and partial density of states analyses. The TDOS plot of a pure VSe_2 monolayer is specified in Figure 3a. To determine the magnetic behavior, spin-up and spin-down states are plotted. It is observed from the figure that the pure material is magnetic due to the asymmetry in spin states. The existence of the density of states at the fermi level implies the metallic behavior of the materials, consistent with earlier findings [64,65]. The total density of states enhanced by the adsorption of the NH_3 molecule on VSe_2 is shown in Figure 5a. In the case of the $VSe_2(Se_v)$ system, an enhancement in TDOS is observed below the Fermi level, as depicted in Figure 5b. The enhancement in the density of states occurs due to the unbound V-atom bonds after the removal of the Se atom from the monolayer. The change in the density of states with the adsorption of NH_3 supports the orbital interactions. The density of states is also enhanced at the fermi level with the adsorption of NH_3 on the $VSe_2(Se_v)$ system.

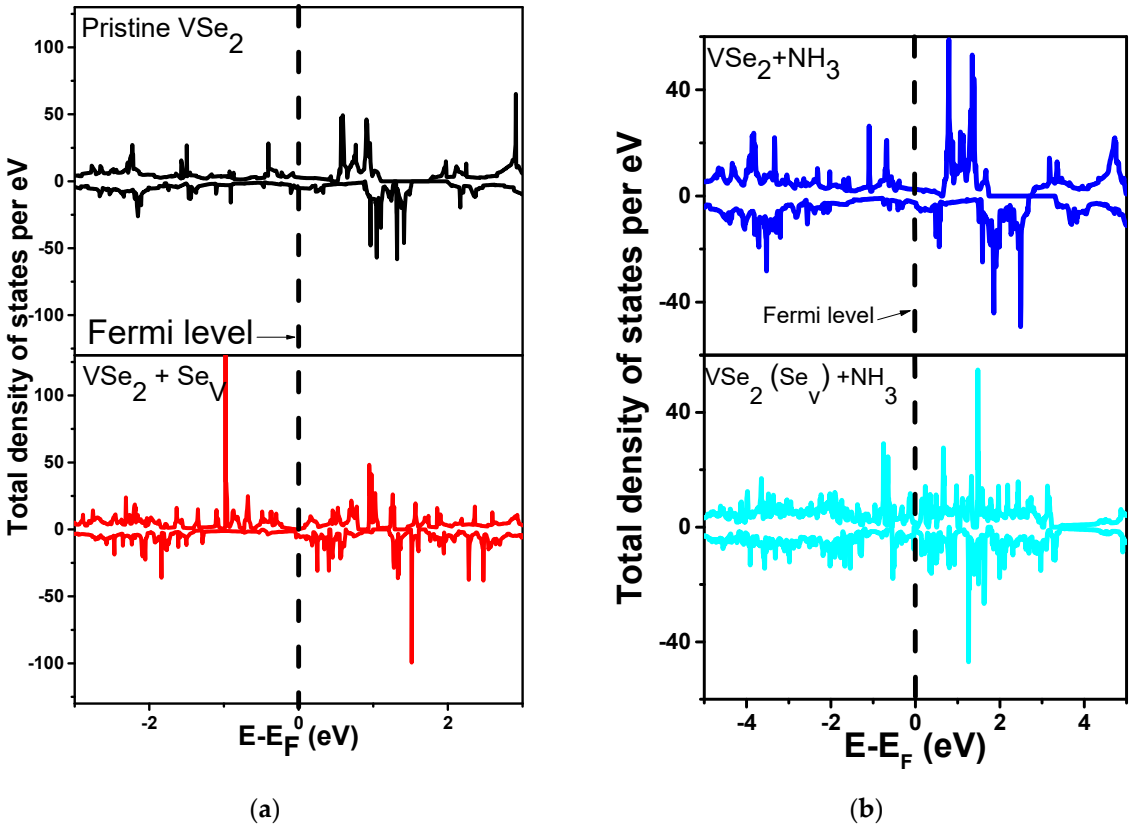

(**a**) (**b**)

Figure 5. Comparison of TDOS plots between (**a**) Pristine VSe_2 and VSe_2 with Se Vacancy, and (**b**) NH_3 adsorbed on pristine VSe_2 on V atom, and NH_3 adsorbed on VSe_2 with Se vacancy on V atom.

3.4. Partial Density of States (PDOS) Plots

To investigate the orbital interactions, the spin-polarized partial density of states (PDOS) is analyzed. The spin-polarized partial density of states (PDOS) for N-2p and H-1s orbitals in NH_3 and $VSe_2(Se_v)$ + NH_3 were computed and are shown in Figure 6a. In the case of the NH_3 molecule, the partial density of states for N-2p and H-1s orbitals is spotted in the valence band. These partial densities of states disappeared (or were reduced) with the adsorption of NH_3 on the $VSe_2(Se_v)$ monolayer. Further, the spin-polarized partial density of states (PDOS) of V-3d orbitals for $VSe_2 + Se_v$ and $VSe_2(Se_v)$ + NH_3 were computed and are shown in Figure 6b. On comparing the PDOS of V-3d orbitals of $VSe_2(Se_v)$ and $VSe_2(Se_v)$ + NH_3 systems, it can be observed that the densities of states are enhanced in the

latter with the adsorption of the NH_3 molecule. This suggests that the monolayer is acting as an electron acceptor, whereas NH_3 is acting as an electron donor. So, we can say that there is a charge transfer from NH_3 to $VSe_2(Se_v)$ due to the adsorption of NH_3.

The total density of states and partial density of states plots have shown that the electronic properties of the VSe_2 monolayer can be tuned with the defect induction, which impacts the adsorption properties.

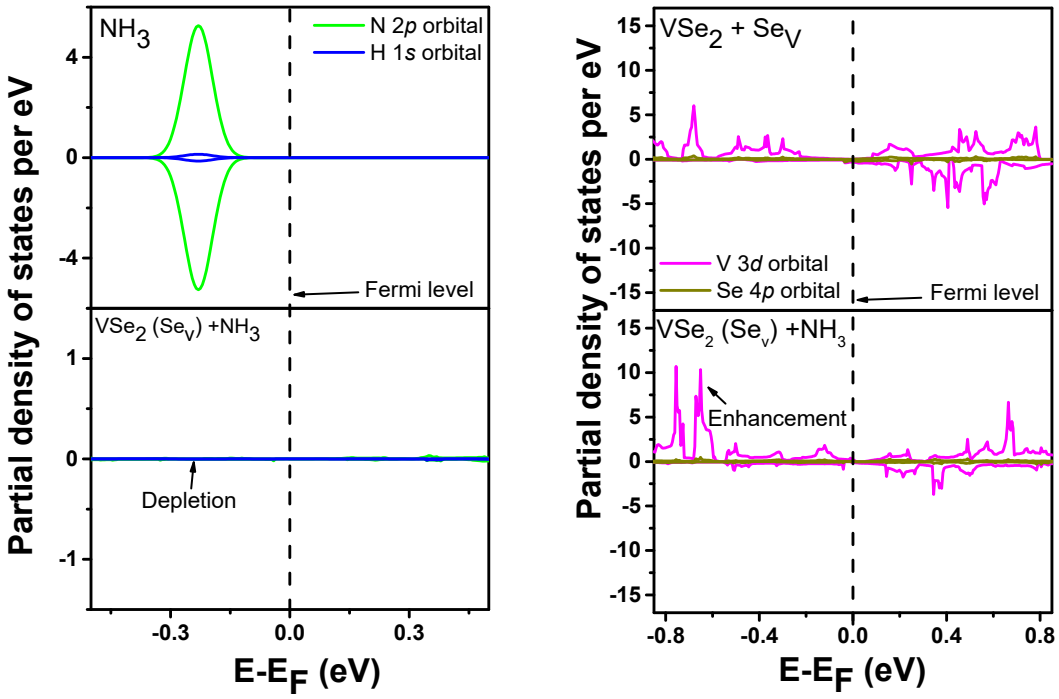

(**a**) (**b**)

Figure 6. PDOS plots for (**a**) N 2p and H 1s orbital in NH_3 and NH_3+ VSe_2 with Se vacancy and (**b**) V 3d and Se 4p orbital in VSe_2 with Se vacancy and NH_3+ VSe_2 with Se vacancy.

3.5. Charge Transfer Analysis

The interactions between the analyte and host were determined in terms of Bader charge analysis [82]. The $VSe_2(Se_v)$ monolayer shows a net gain of 0.009e of charge due to adsorption of the NH_3 molecule whereas, the NH_3 molecule shows a net loss of 0.009e of charge, suggesting that the monolayer acts as an electron acceptor. The Bader charge analysis is in accordance with the partial density of states (PDOS) plots (Figure 6). The above observation is consistent with the opinion of earlier researchers regarding ammonia sensing in terms of charge transfer course. (Table 2) [37, 83–86]. Additionally, a charge density difference plot has been shown in Figure 7. It is performed with the relation:

$$\rho_{Difference} = \rho_{VSe_2(Se_V)+NH_3} - \rho_{VSe_2(Se_V)} - \rho_{NH_3}$$

For all three systems, the ISO values are around 0.04e, wherein red regions denote regions of charge loss and green or blue regions denote charge gain. In all three systems, a charge loss region is noted around the N atom of the NH_3 molecule, while a charge gain region is noted over the VSe_2 surface with a Se vacancy.

Table 2. comparison with earlier reported charge transfer data for NH_3 sensing.

2D Material	Charge Lost by NH_3	Reference
MoS_2/ WS_2	0.09e/0.03e	[37]
Ag_3-WSe_2 monolayer	0.202e	[83]
MoS_2	Pictorial illustration	[84]

$Ti_3C_2T_x$ MXene @ TiO_2/MoS_2 heterostructure	~0.03e	[85]
WOS nanosheet	Pictorial illustration	[86]
$VSe_2(Se_v)$	0.009e	This work

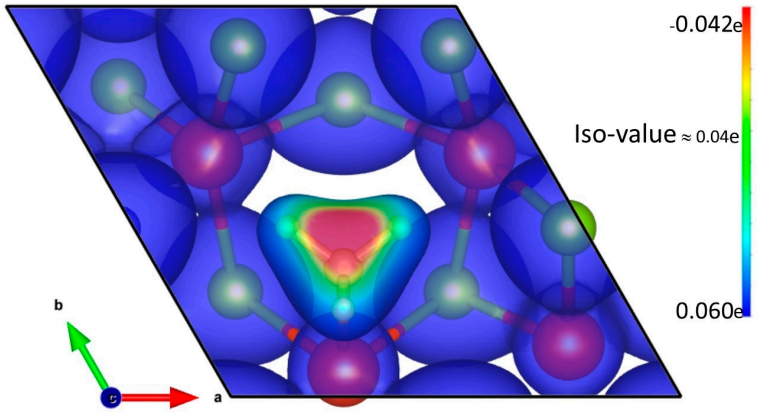

Figure 7. The charge density difference plot of NH_3-attached Se-deficient VSe_2. Red regions indicate charge loss, whereas blue and green regions indicate charge gain.

3.6. Thermal Stability from Molecular Dynamics Simulations

A nanosensor should be stable at higher temperatures for its efficient performance. Moreover, the gas molecules adsorbed on it should remain intact in the system until the sensing procedure is completed. As pristine VSe_2 is a synthesized material, it is thermally stable at room temperature. So, we have investigated the thermal stability of $VSe_2 + NH_3$ and $VSe_2(Se_v) + NH_3$ systems. The ab initio molecular dynamics simulations were carried out to investigate the thermal stability of the considered material at higher temperatures. The snapshots of equilibrated $VSe_2 + NH_3$ and $VSe_2(Se_v) + NH_3$ systems after 5 ps at 400 K are shown in Figure 8.

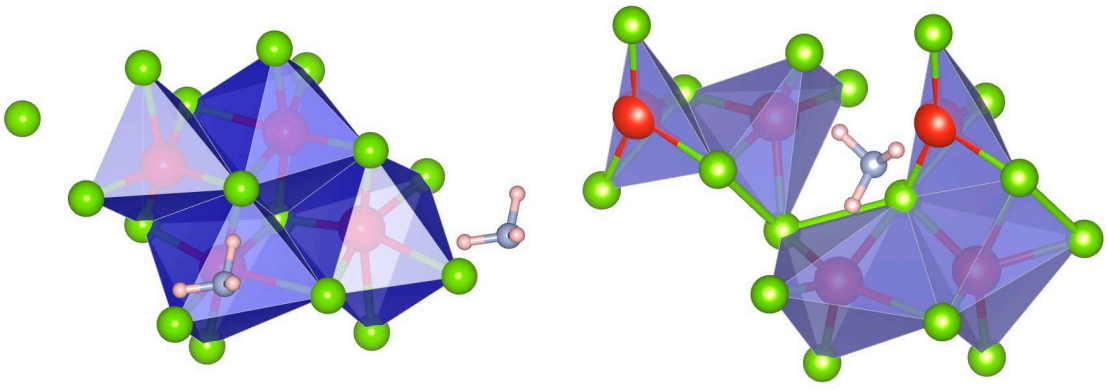

(**a**) (**b**)

Figure 8. MD snapshots (**a**) $VSe_2 + NH_3$ (**b**) $VSe_2(Se_v) + NH_3$ at 400 K after 5 ps; for the pristine VSe_2: as adsorption energy is less, NH_3 is desorbed while for VSe_2 (Se_v) it remains intact.

The bond length fluctuations (between N of NH_3 and V of VSe_2) with the temperature are plotted in Figure 9. We can notice that for pristine VSe_2, the NH_3 molecule goes away from the system starting with a temperature of 108 K. It seems that the NH_3 molecule desorbs from the system once the temperature is increased, with desorption starting around 108 K. This is because NH_3 is bonded very weakly on pristine VSe_2 and goes out of the system at higher temperatures. So NH_3 desorbs from the system below room temperature for pristine VSe_2. So, pristine VSe_2 is not suitable for NH_3 sensing due to weaker interactions and low adsorption energy. But for $VSe_2(Se_v) + NH_3$ system, the bond length

fluctuations are not much. It is around 10% of the mean value, suggesting that adsorbed NH_3 remains intact at 300 K and even up to 400 K on the sensing material. This is due to the fact that the adsorption energy of NH_3 on defected VSe_2 has increased from −0.12 eV for the pristine system to −0.97 eV for the $VSe_2(Se_v)$ system. Strong adsorption energy is due to charge transfer from NH_3 to defected VSe_2. So, the defected VSe_2 is promising for NH_3 sensing.

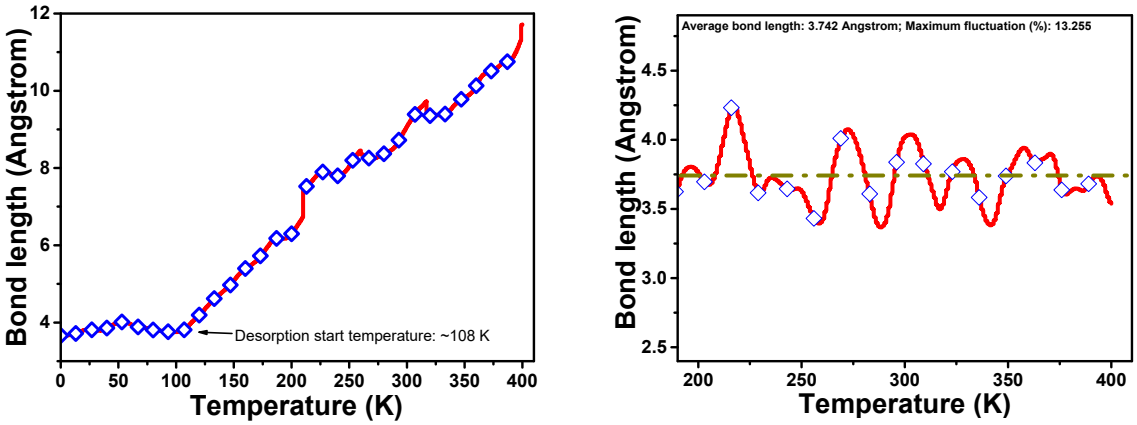

(**a**) (**b**)

Figure 9. Variation of bond length N-V with the temperature during AIMD simulations for (**a**) VSe_2 + NH_3 (**b**) $VSe_2(Se_v)$ + NH_3; for pristine VSe_2, NH_3 is desorbed while for $VSe_2(Se_v)$ it remains intact.

3.7. Recovery Time (τ)

The reversible sensors could be used repeatedly and hence, are economically convenient for utilization in industrial sectors [65]. The recovery time analysis helps to determine the extent to which a sensor can be used reversibly. The recovery time determines the time required for an analyte to desorb from the host surface. It can be computed using the following equation [65]:

$$\tau = \nu^{-1}\exp(-E_{ads}/kT) \quad (2)$$

In the equation, the ν denotes the frequency factor or the reciprocal of the pre-exponential factor of the Arrhenius equation [87]. The terms E_{ads}, k, and T denote the adsorption energy, Boltzmann constant, and temperature, respectively.

Using this equation, the recovery time for VSe_2 + NH_3 and $VSe_2(Se_v)$ + NH_3 systems were computed at 300 K and 500 K for visible yellow light and UV light. The τ values are shown in Table 3. The tabulated values show that at 300 K under UV radiation, $VSe_2(Se_v)$ + NH_3 system promises a convenient recovery time (~2 s). This suggests that $VSe_2(Se_v)$ + NH_3 system can act as a reusable sensor.

Table 3. Recovery time for VSe_2 + NH_3 and $VSe_2(Se_v)$ + NH_3 systems at 300 K and 500 K for yellow light and UV light.

System	Recovery Time (s)			
	Yellow Light (ν = ~5.2 × 10^{14} Hz)		UV Radiation (ν = 1 × 10^{14} Hz)	
	300 K	500 K	300 K	500 K
VSe_2 + NH_3 (with VdW)	1.97 × 10^{-13}	3.09 × 10^{-14}	1.02 × 10^{-14}	1.61 × 10^{-15}
$VSe_2(Se_v)$ + NH_3 (with VdW)	1.92 × 10^{-15}	1.16 × 10^{-05}	*1.99*	6.01 × 10^{-07}

Apart from the above, response time is also considered a very important parameter for determining the sensitivity of any gas detector. When the gas is initially applied, it

takes a few seconds for the sensor output current to attain steady-state conditions [88]. The response time of the sensor is commonly specified by the T_{90} or T_{50} time. T_{90} is the time for the sensor's response current to reach 90% of its steady-state value. Similarly, the T_{50} metric is the time required for the sensor to reach 50% of its steady-state value [88]. Future progress in this work can consist of determining the response time for VSe_2 to detect NH_3.

In spite of promising results, improvements in 2D VSe_2 are needed to attain better sensitivity, selectivity, and stability. Specifically, there is scope for improvement in recovery time owing to the slow gas desorption process to enable it suitable for usage at room temperature. Currently, this kind of resource seems to be substandard in terms of sensing presentations when contrasted with metal oxide nanostructures; however, their performance is on par with that of pristine graphene. The technology available as of now to physically fabricate planer structures is still not industrially budget-friendly, so more technological advancement is necessary.

4. Conclusions

The structural, electronic, and sensing properties of pure and defected VSe_2 monolayers have been investigated with density functional theory calculations. The energetic stability of $VSe_2(Se_v)$ + NH_3 and $VSe_2(V_v)$ + NH_3 monolayers is studied as adsorption energy values. The $VSe_2(Se_v)$ binds strongly with the adsorbed NH_3 molecule compared to the pure nanomaterial. With the introduction of Se vacancy, the adsorption energy increases from −0.12 eV in the pristine case to −0.97 eV for $VSe_2(Se_v)$. Charge transfer from NH_3 to defected VSe_2 is responsible for stronger adsorption. It has been observed that NH_3 acts as a charge donor and the host, i.e., VSe_2, as a charge acceptor to cause the adsorption to be effective. The thermal stability of the $VSe_2(Se_v)$ + NH_3 system was investigated by performing ab initio molecular dynamics simulations at 300 K and 400 K and the system was found to be structurally stable even at higher temperatures. The recovery time analysis suggests that the $VSe_2(Se_v)$ monolayer can act as a reusable nanosensor. The present studies show that the sensing properties of the VSe_2 monolayer can be significantly improved with the introduction of Se-defects in the lattice structure. Or, in other words, tuning structural and electronic properties through the introduction of Se vacancy aids in enhancing the sensing properties of the VSe_2 monolayer for NH_3 adsorption. The obtained results will be potentially helpful for experimentalists to design defect-engineered TMD-based novel gas sensors.

Supplementary Materials: The following supporting information can be downloaded at: https://www.mdpi.com/article/10.3390/bios13020257/s1, Table S1: Adsorption energies for the adsorption of NH3 on VSe2 at different sites;

Author Contributions: G.S. software, writing and editing draft, making illustrations; S.P.K. writing original draft; C.S.R. support and supervision; B.C. conceptualization, software, editing draft, and overall supervision. All authors have read and agreed to the published version of the manuscript.

Funding: This research received no external funding.

Institutional Review Board Statement: Not applicable.

Informed Consent Statement: Not applicable.

Data Availability Statement: The data presented in this study are available on reasonable request to the corresponding author.

Acknowledgments: B.C. would like to thank Nandini Garg, T. Sakuntala, S. M. Yusuf, and A. K. Mohanty for their encouragement and support and the staff of the computer division of BARC for availing facility for supercomputing.

Conflicts of Interest: The authors declare no conflict of interest.

References

1. Kong, J.; Franklin, N.R.; Zhou, C.; Chapline, M.G.; Peng, S.; Cho, K.; Dai, H. Nanotube molecular wires as chemical sensors. *Science* **2000**, *287*, 622–625.
2. Mirzaei, A.; Lee, J.-H.; Majhi, S.M.; Weber, M.; Bechelany, M.; Kim, H.W.; Kim, S.S. Resistive gas sensors based on metal-oxide nanowires. *J. Appl. Phys.* **2019**, *126*, 241102.
3. Chen, X.; Wong, C.K.Y.; Yuan, C.A.; Zhang, G. Nanowire-based gas sensors. *Sens. Actuators B Chem.* **2013**, *177*, 178–195.
4. Sun, Y.; Chen, L.; Zhang, F.; Li, D.; Pan, H.; Ye, J. First-principles studies of HF molecule adsorption on intrinsic graphene and Al-doped graphene. *Solid State Commun.* **2010**, *150*, 1906–1910.
5. Zhang, J.; Qin, Z.; Zeng, D.; Xie, C. Metal-oxide-semiconductor based gas sensors: Screening, preparation, and integration. *Phys. Chem. Chem. Phys.* **2017**, *19*, 6313–6329.
6. Wang, C.; Yin, L.; Zhang, L.; Xiang, D.; Gao, R. Metal oxide gas sensors: Sensitivity and influencing factors. *Sensors* **2010**, *10*, 2088–2106.
7. Cai, Z.; Liu, B.; Zou, X.; Cheng, H.-M. Chemical vapor deposition growth and applications of two-dimensional materials and their heterostructures. *Chem. Rev.* **2018**, *118*, 6091–6133.
8. Hussain, T.; Hankel, M.; Searles, D.J. Improving sensing of sulfur-containing gas molecules with ZnO monolayers by implanting dopants and defects. *J. Phys. Chem. C* **2017**, *121*, 24365–24375.
9. Oudenhoven, J.F.M.; Knoben, W.; Van Schaijk, R. Electrochemical detection of ammonia using a thin ionic liquid film as the electrolyte. *Procedia Eng.* **2015**, *120*, 983–986.
10. Amirjani, A.; Fatmehsari, D.H. Colorimetric detection of ammonia using smartphones based on localized surface plasmon resonance of silver nanoparticles. *Talanta* **2018**, *176*, 242–246.
11. Arya, S.; Riyas, M.; Sharma, A.; Singh, B.; Prerna; Bandhoria, P.; Khan, S.; Bharti, V. Electrochemical detection of ammonia solution using tin oxide nanoparticles synthesized via sol–gel route. *Appl. Phys. A* **2018**, *124*, 538.
12. Ben Aziza, Z.; Zhang, Q.; Baillargeat, D. Graphene/mica based ammonia gas sensors. *Appl. Phys. Lett.* **2014**, *105*, 254102.
13. Geim, A.K., Novoselov, K.S. The rise of graphene. In *Nanoscience and Technology: A Collection of Reviews from Nature Journals*; World Scientific: Singapore 2010; pp. 11–19.
14. Radisavljevic, B.; Radenovic, A.; Brivio, J.; Giacometti, V.; Kis, A. Single-layer MoS_2 transistors. *Nat. Nanotechnol.* **2011**, *6*, 147–150.
15. Hussain, T.; De Sarkar, A.; Ahuja, R. Functionalization of hydrogenated graphene by polylithiated species for efficient hydrogen storage. *Int. J. Hydrog. Energy* **2014**, *39*, 2560–2566.
16. Yagmurcukardes, M.; Peeters, F.M. Stable single layer of Janus MoSO: Strong out-of-plane piezoelectricity. *Phys. Rev. B* **2020**, *101*, 155205.
17. Yagmurcukardes, M.; Qin, Y.; Ozen, S.; Sayyad, M.; Peeters, F.M.; Tongay, S.; Sahin, H. Quantum properties and applications of 2D Janus crystals and their superlattices. *Appl. Phys. Rev.* **2020**, *7*, 011311.
18. Li, L.L.; Bacaksiz, C.; Nakhaee, M.; Pentcheva, R.; Peeters, F.M.; Yagmurcukardes, M. Single-layer Janus black arsenic-phosphorus (b-AsP): Optical dichroism, anisotropic vibrational, thermal, and elastic properties. *Phys. Rev. B* **2020**, *101*, 134102.
19. Wang, T.; Huang, D.; Yang, Z.; Xu, S.; He, G.; Li, X.; Hu, N.; Yin, G.; He, D.; Zhang, L. A review on graphene-based gas/vapor sensors with unique properties and potential applications. *Nano-Micro Lett.* **2016**, *8*, 95–119.
20. Nag, A.; Mitra, A.; Mukhopadhyay, S.C. Graphene and its sensor-based applications: A review. *Sens. Actuators A Phys.* **2018**, *270*, 177–194.
21. Yang, S.; Jiang, C.; Wei, S.-H. Gas sensing in 2D materials. *Appl. Phys. Rev.* **2017**, *4*, 021304.
22. Pospischil, A.; Furchi, M.M.; Mueller, T. Solar-energy conversion and light emission in an atomic monolayer p–n diode. *Nat. Nanotechnol.* **2014**, *9*, 257–261.
23. Shukla, V.; Wärnå, J.; Jena, N.K.; Grigoriev, A.; Ahuja, R. Toward the realization of 2D borophene based gas sensor. *J. Phys. Chem. C* **2017**, *121*, 26869–26876.
24. Huang, C.-S.; Murat, A.; Babar, V.; Montes, E.; Schwingenschlögl, U. Adsorption of the Gas Molecules NH3, NO, NO2, and CO on Borophene. *J. Phys. Chem. C* **2018**, *122*, 14665–14670.
25. Shen, J.; Yang, Z.; Wang, Y.; Xu, L.-C.; Liu, R.; Liu, X. Organic gas sensing performance of the borophene van der Waals heterostructure. *J. Phys. Chem. C* **2020**, *125*, 427–435.
26. Babar, V.; Sharma, S.; Schwingenschlögl, U. Gas sensing performance of pristine and monovacant C6BN monolayers evaluated by density functional theory and the nonequilibrium green's function formalism. *J. Phys. Chem. C* **2020**, *124*, 5853–5860.
27. Gupta, S.K.; Singh, D.; Rajput, K.; Sonvane, Y. Germanene: A new electronic gas sensing material. *RSC Adv.* **2016**, *6*, 102264–102271.
28. Song, Z.; Ang, W.L.; Sturala, J.; Mazanek, V.; Marvan, P.; Sofer, Z.; Ambrosi, A.; Ding, C.; Luo, X.; Bonanni, A. Functionalized germanene-based nanomaterials for the detection of single nucleotide polymorphism. *ACS Appl. Nano Mater.* **2021**, *4*, 5164–5175.
29. Sosa, A.N.; Santana, J.E.; Miranda, Á.; Pérez, L.A.; Trejo, A.; Salazar, F.; Cruz-Irisson, M. NH_3 capture and detection by metal-decorated germanene: A DFT study. *J. Mater. Sci.* **2022**, *57*, 8516–8529.
30. Xu, K.; Liao, N.; Zheng, B.; Zhou, H. Adsorption and diffusion behaviors of H_2, H_2S, NH_3, CO and H_2O gases molecules on MoO_3 monolayer: A DFT study. *Phys. Lett. A* **2020**, *384*, 126533.

31. Qu, Y.; Ding, J.; Fu, H.; Peng, J.; Chen, H. Adsorption of CO, NO, and NH_3 on ZnO monolayer decorated with noble metal (Ag, Au). *Appl. Surf. Sci.* **2020**, *508*, 145202.
32. Lv, Y.; Wang, Y.; Zhang, H.; Dai, C. Adsorption of NH_3 and NO_2 molecules on the carbon doped C3N monolayer: A first principles study. *Comput. Theor. Chem.* **2021**, *1195*, 113075.
33. Kou, L.; Du, A.; Chen, C.; Frauenheim, T. Strain engineering of selective chemical adsorption on monolayer MoS_2. *Nanoscale* **2014**, *6*, 5156–5161.
34. He, Q.; Zeng, Z.; Yin, Z.; Li, H.; Wu, S.; Huang, X.; Zhang, H. Fabrication of flexible MoS2 thin-film transistor arrays for practical gas-sensing applications. *Small* **2012**, *8*, 2994–2999.
35. Kim, S.; Konar, A.; Hwang, W.-S.; Lee, J.H.; Lee, J.; Yang, J.; Jung. C.; Kim, H.; Yoo, J.-B.; Choi, J.-Y.; et al. High-mobility and low-power thin-film transistors based on multilayer MoS2 crystals. *Nat. Commun.* **2012**, *3*, 1011.
36. Radisavljevic, B.; Whitwick, M.B.; Kis, A. Integrated circuits and logic operations based on single-layer MoS_2. *ACS Nano* **2011**, *5*, 9934–9938.
37. Babar, V.; Vovusha, H.; Schwingenschlögl, U. Density functional theory analysis of gas adsorption on monolayer and few layer transition metal dichalcogenides: Implications for sensing. *ACS Appl. Nano Mater.* **2019**, *2*, 6076–6080.
38. Abbasi, A.; Sardroodi, J.J. Adsorption of O_3, SO_2 and SO_3 gas molecules on MoS_2 monolayers: A computational investigation. *Appl. Surf. Sci.* **2019**, *469*, 781–791.
39. Deng, X.; Liang, X.; Ng, S.-P.; Wu, C.-M.L. Adsorption of formaldehyde on transition metal doped monolayer MoS_2: A DFT study. *Appl. Surf. Sci.* **2019**, *484*, 1244–1252.
40. Nayeri, M.; Moradinasab, M.; Fathipour, M. The transport and optical sensing properties of MoS_2, $MoSe_2$, WS_2 and WSe_2 semiconducting transition metal dichalcogenides. *Semicond. Sci. Technol.* **2018**, *33*, 025002.
41. Abbas, H.G.; Debela, T.T.; Hussain, S.; Hussain, I. Inorganic molecule (O_2, NO) adsorption on nitrogen-and phosphorus-doped MoS_2 monolayer using first principle calculations. *RSC Adv.* **2018**, *8*, 38656–38666.
42. Cabral, L.; Sabino, F.P.; Lima, M.P.; Marques, G.E.; Lopez-Richard, V.; Da Silva, J.L.F. Azobenzene Adsorption on the MoS_2(0001) Surface: A Density Functional Investigation within van der Waals Corrections. *J. Phys. Chem. C* **2018**, *122*, 18895–18901.
43. Ma, D.; Ma, B.; Lu, Z.; He, C.; Tang, Y.; Lu, Z.; Yang, Z. Interaction between H_2O, N_2, CO, NO, NO_2 and N_2O molecules and a defective WSe_2 monolayer. *Phys. Chem. Chem. Phys.* **2017**, *19*, 26022–26033.
44. Idrees, M.; Din, H.U.; Ali, R.; Rehman, G.; Hussain, T.; Nguyen, C.V.; Ahmad, I.; Amin, B. Optoelectronic and solar cell applications of Janus monolayers and their van der Waals heterostructures. *Phys. Chem. Chem. Phys.* **2019**, *21*, 18612–18621.
45. Ma, X.; Wu, X.; Wang, H.; Wang, Y. A Janus MoSSe monolayer: A potential wide solar-spectrum water-splitting photocatalyst with a low carrier recombination rate. *J. Mater. Chem. A* **2018**, *6*, 2295–2301.
46. Jin, C.; Tang, X.; Tan, X.; Smith, S.C.; Dai, Y.; Kou, L. A Janus MoSSe monolayer: A superior and strain-sensitive gas sensing material. *J. Mater. Chem. A* **2019**, *7*, 1099–1106.
47. Shang, C.; Lei, X.; Hou, B.; Wu, M.; Xu, B.; Liu, G.; Ouyang, C. Theoretical prediction of Janus MoSSe as a potential anode material for lithium-ion batteries. *J. Phys. Chem. C* **2018**, *122*, 23899–23909.
48. Dong, L.; Lou, J.; Shenoy, V.B. Large in-plane and vertical piezoelectricity in Janus transition metal dichalchogenides. *ACS Nano* **2017**, *11*, 8242–8248.
49. Li, Y.; Wang, J.; Zhou, B.; Wang, F.; Miao, Y.; Wei, J.; Zhang, B.; Zhang, K. Tunable interlayer coupling and Schottky barrier in graphene and Janus MoSSe heterostructures by applying an external field. *Phys. Chem. Chem. Phys.* **2018**, *20*, 24109–24116.
50. Kaur, S.P.; Kumar, T.J.D. Tuning structure, electronic, and catalytic properties of non-metal atom doped Janus transition metal dichalcogenides for hydrogen evolution. *Appl. Surf. Sci.* **2021**, *552*, 149146.
51. Chaurasiya, R.; Dixit, A. Defect engineered MoSSe Janus monolayer as a promising two dimensional material for NO_2 and NO gas sensing. *Appl. Surf. Sci.* **2019**, *490*, 204–219.
52. Sanyal, G.; Vaidyanathan, A.; Rout, C.S.; Chakraborty, B. Recent developments in two-dimensional layered tungsten dichalcogenides based materials for gas sensing applications. *Mater. Today Commun.* **2021**, *28*, 102717.
53. Shankar, P.; Rayappan, J.B.B. Gas sensing mechanism of metal oxides: The role of ambient atmosphere, type of semiconductor and gases-A review. *Sci. Lett. J.* **2015**, *4*, 126.
54. Yuan, H.T.; Toh, M.; Morimoto, K.; Tan, W.; Wei, F.; Shimotani, H.; Kloc, C.; Iwasa, Y. Liquid-gated electric-double-layer transistor on layered metal dichalcogenide, SnS_2. *Appl. Phys. Lett.* **2011**, *98*, 012102.
55. Pu, J.; Yomogida, Y.; Liu, K.-K.; Li, L.-J.; Iwasa, Y.; Takenobu, T. Highly flexible MoS_2 thin-film transistors with ion gel dielectrics. *Nano Lett.* **2012**, *12*, 4013–4017.
56. Xie, J.; Zhang, J.; Li, S.; Grote, F.; Zhang, X.; Zhang, H.; Wang, R.; Lei, Y.; Pan, B.; Xie, Y. Controllable disorder engineering in oxygen-incorporated MoS2 ultrathin nanosheets for efficient hydrogen evolution. *J. Am. Chem. Soc.* **2013**, *135*, 17881–17888.
57. Liu, P.; Zhu, J.; Zhang, J.; Xi, P.; Tao, K.; Gao, D.; Xue, D. P dopants triggered new basal plane active sites and enlarged interlayer spacing in MoS_2 nanosheets toward electrocatalytic hydrogen evolution. *ACS Energy Lett.* **2017**, *2*, 745–752.
58. Suh, J.; Park, T.-E.; Lin, D.-Y.; Fu, D.; Park, J.; Jung, H.J.; Chen, Y.; Ko, C.; Jang, C.; Sun, Y.; et al. Doping against the native propensity of MoS_2: Degenerate hole doping by cation substitution. *Nano Lett.* **2014**, *14*, 6976–6982.
59. Choi, S.Y.; Kim, Y.; Chung, H.-S.; Kim, A.R.; Kwon, J.-D.; Park, J.; Kim, Y.L.; Kwon, S.-H.; Hahm, M.G.; Cho, B. Effect of Nb doping on chemical sensing performance of two-dimensional layered $MoSe_2$. *ACS Appl. Mater. Interfaces* **2017**, *9*, 3817–3823.

60. Panigrahi, P.; Hussain, T.; Karton, A.; Ahuja, R. Elemental substitution of two-dimensional transition metal dichalcogenides ($MoSe_2$ and $MoTe_2$): Implications for enhanced gas sensing. *ACS Sens.* **2019**, *4*, 2646–2653.
61. Zhu, J.; Zhang, H.; Tong, Y.; Zhao, L.; Zhang, Y.; Qiu, Y.; Lin, X. First-principles investigations of metal (V, Nb, Ta)-doped monolayer MoS_2: Structural stability, electronic properties and adsorption of gas molecules. *Appl. Surf. Sci.* **2017**, *419*, 522–530.
62. Luo, H.; Cao, Y.; Zhou, J.; Feng, J.; Cao, J.; Guo, H. Adsorption of NO_2, NH_3 on monolayer MoS_2 doped with Al, Si, and P: A first-principles study. *Chem. Phys. Lett.* **2016**, *643*, 27–33.
63. Kaur, S.P.; Hussain, T.; Kumar, T.J.D. Substituted 2D Janus WSSe monolayers as efficient nanosensor toward toxic gases. *J. Appl. Phys.* **2021**, *130*, 014501.
64. Sanyal, G.; Lakshmy, S.; Vaidyanathan, A.; Kalarikkal, N.; Chakraborty, B. Detection of nitrobenzene in pristine and metal decorated 2D dichalcogenide VSe_2: Perspectives from density functional theory. *Surf. Interfaces* **2022**, *29*, 101816.
65. Chakraborty, B.; Vaidyanathan, A.; Sanyal, G.; Lakshmy, S.; Kalarikkal, N. Transition metal decorated VSe_2 as promising catechol sensor: Insights from DFT simulations. *J. Appl. Phys.* **2022**, *132*, 084502.
66. Liu, Y.; Xiao, C.; Li, Z.; Xie, Y. Vacancy engineering for tuning electron and phonon structures of two-dimensional materials. *Adv. Energy Mater.* **2016**, *6*, 1600436.
67. Zhang, C.; Liu, G.; Geng, X.; Wu, K.; Debliquy, M. Metal oxide semiconductors with highly concentrated oxygen vacancies for gas sensing materials: A review. *Sens. Actuators A Phys.* **2020**, *309*, 112026.
68. Al-Hashem, M.; Akbar, S.; Morris, P. Role of oxygen vacancies in nanostructured metal-oxide gas sensors: A review. *Sens. Actuators B Chem.* **2019**, *301*, 126845.
69. Guo, X.; Shi, Y.; Ding, Y.; He, Y.; Du, B.; Liang, C.; Tan, Y.; Liu, P.; Miao, X.; He, Y.; et al. Indium-doping-induced selenium vacancy engineering of layered tin diselenide for improving room-temperature sulfur dioxide gas sensing. *J. Mater. Chem. A* **2022**, *10*, 22629–22637.
70. Qin, Z.; Xu, K.; Yue, H.; Wang, H.; Zhang, J.; Ouyang, C.; Xie, C.; Zeng, D. Enhanced room-temperature NH3 gas sensing by 2D SnS2 with sulfur vacancies synthesized by chemical exfoliation. *Sens. Actuators B Chem.* **2018**, *262*, 771–779.
71. Xia, Y.; Hu, C.; Guo, S.; Zhang, L.; Wang, M.; Peng, J.; Xu, L.; Wang, J. Sulfur-vacancy-enriched MoS2 nanosheets based heterostructures for near-infrared optoelectronic NO_2 sensing. *ACS Appl. Nano Mater.* **2019**, *3*, 665–673.
72. Norouzzadeh, E.; Mohammadi, S.; Moradinasab, M. First principles characterization of defect-free and vacancy-defected monolayer $PtSe_2$ gas sensors. *Sens. Actuators A Phys.* **2020**, *313*, 112209.
73. Chen, D.; Zhang, X.; Xiong, H.; Li, Y.; Tang, J.; Xiao, S.; Zhang, D. A first-principles study of the SF_6 decomposed products adsorbed over defective WS_2 monolayer as promising gas sensing device. *IEEE Trans. Device Mater. Reliab.* **2019**, *19*, 473–483.
74. Kresse, G.; Furthmüller, J. Efficiency of ab-initio total energy calculations for metals and semiconductors using a plane-wave basis set. *Comput. Mater. Sci.* **1996**, *6*, 15–50.
75. Kresse, G.; Furthmüller, J. Efficient iterative schemes for ab initio total-energy calculations using a plane-wave basis set. *Phys. Rev. B* **1996**, *54*, 11169.
76. Kresse, G.; Hafner, J. Ab initio molecular-dynamics simulation of the liquid-metal–amorphous-semiconductor transition in germanium. *Phys. Rev. B* **1994**, *49*, 14251.
77. Kresse, G.; Hafner, J. Ab initio molecular dynamics for liquid metals. *Phys. Rev. B* **1993**, *47*, 558.
78. Perdew, J.P.; Burke, K.; Ernzerhof, M. Generalized gradient approximation made simple. *Phys. Rev. Lett.* **1996**, *77*, 3865.
79. Grimme, S.; Antony, J.; Ehrlich, S.; Krieg, H. A consistent and accurate ab initio parametrization of density functional dispersion correction (DFT-D) for the 94 elements H-Pu. *J. Chem. Phys.* **2010**, *132*, 154104.
80. Grimme, S. Density functional theory with London dispersion corrections. *WIREs Comput. Mol. Sci.* **2011**, *1*, 211–228.
81. Monkhorst, H.J.; Pack, J.D. Special points for Brillouin-zone integrations. *Phys. Rev. B* **1976**, *13*, 5188.
82. Tang, W.; Sanville, E.; Henkelman, G. A grid-based Bader analysis algorithm without lattice bias. *J. Phys. Condens. Matter* **2009**, *21*, 084204.
83. Mi, H.; Zhou, Q.; Zeng, W. A density functional theory study of the adsorption of Cl_2, NH_3, and NO_2 on Ag_3-doped WSe_2 monolayers. *Appl. Surf. Sci.* **2021**, *563*, 150329.
84. Cho, B.; Hahm, M.G.; Choi, M.; Yoon, J.; Kim, A.R.; Lee, Y.-J.; Park, S.-G.; Kwon, J.-D.; Kim, C.S.; Song, M.; et al. Charge-transfer-based gas sensing using atomic-layer MoS_2. *Sci. Rep.* **2015**, *5*, 8052.
85. Tian, X.; Yao, L.; Cui, X.; Zhao, R.; Chen, T.; Xiao, X.; Wang, Y. A two-dimensional $Ti_3C_2T_x$ MXene@TiO_2/MoS_2 heterostructure with excellent selectivity for the room temperature detection of ammonia. *J. Mater. Chem. A* **2022**, *10*, 5505–5519.
86. Zheng, Y.; Sun, L.; Liu, W.; Wang, C.; Dai, Z.; Ma, F. Tungsten oxysulfide nanosheets for highly sensitive and selective NH_3 sensing. *J. Mater. Chem. C* **2020**, *8*, 4206–4214.
87. Arrhenius, S. Über die Dissociationswärme und den Einfluss der Temperatur auf den Dissociationsgrad der Elektrolyte. *Zeitschrift für physikalische Chemie* **1889**, *4*, 96–116.
88. Warburton, P.R.; Pagano, M.P.; Hoover, R.; Logman, M.; Crytzer, K.; Warburton, Y.J. Amperometric gas sensor response times. *Anal. Chem.* **1998**, *70*, 998–1006.